Medical Hyperspectral Imaging:

Artificial Intelligence & Image-Guided Surgery

Baowei Fei, PhD, EngD

Cecil H. and Ida Green Chair in Systems Biology Science
Professor of Bioengineering at UT Dallas
Professor of Radiology at UT Southwestern

Quantitative Bioimaging Laboratory
Center for Imaging and Surgical Innovation (CISI)

www.fei-lab.org

UT DALLAS
The University of Texas at Dallas

UT Southwestern
Medical Center

Hyperspectral Imaging

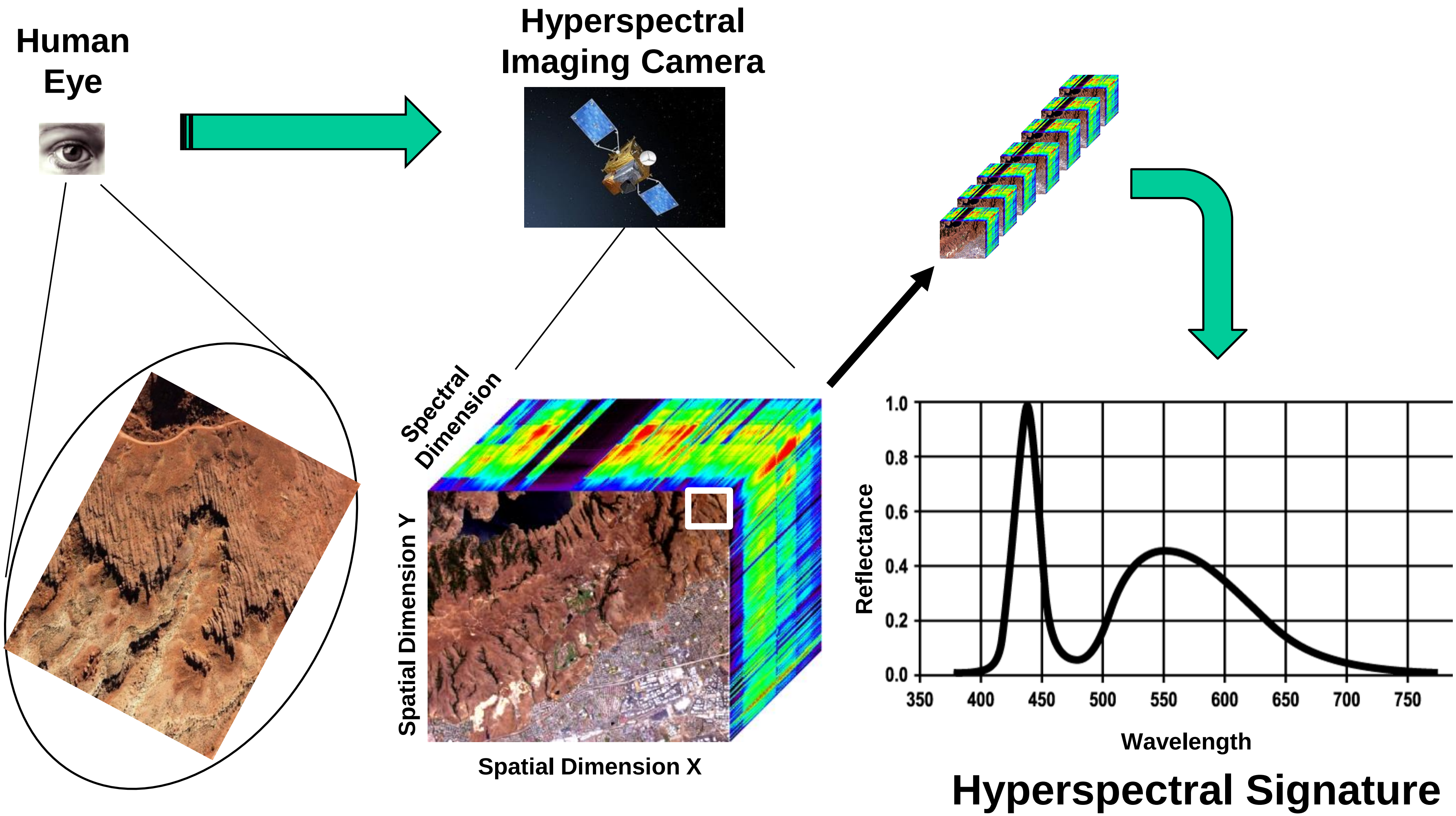

UT DALLAS
The University of Texas at Dallas

UT Southwestern
Medical Center

Hyperspectral imaging records many discrete spectral ‘slices’ of reflected energy across the ***visible and near infrared*** portion of the spectrum, resulting in numerous images of a given target. Individual spectral ‘slices’ contain unique information about the imaged object.

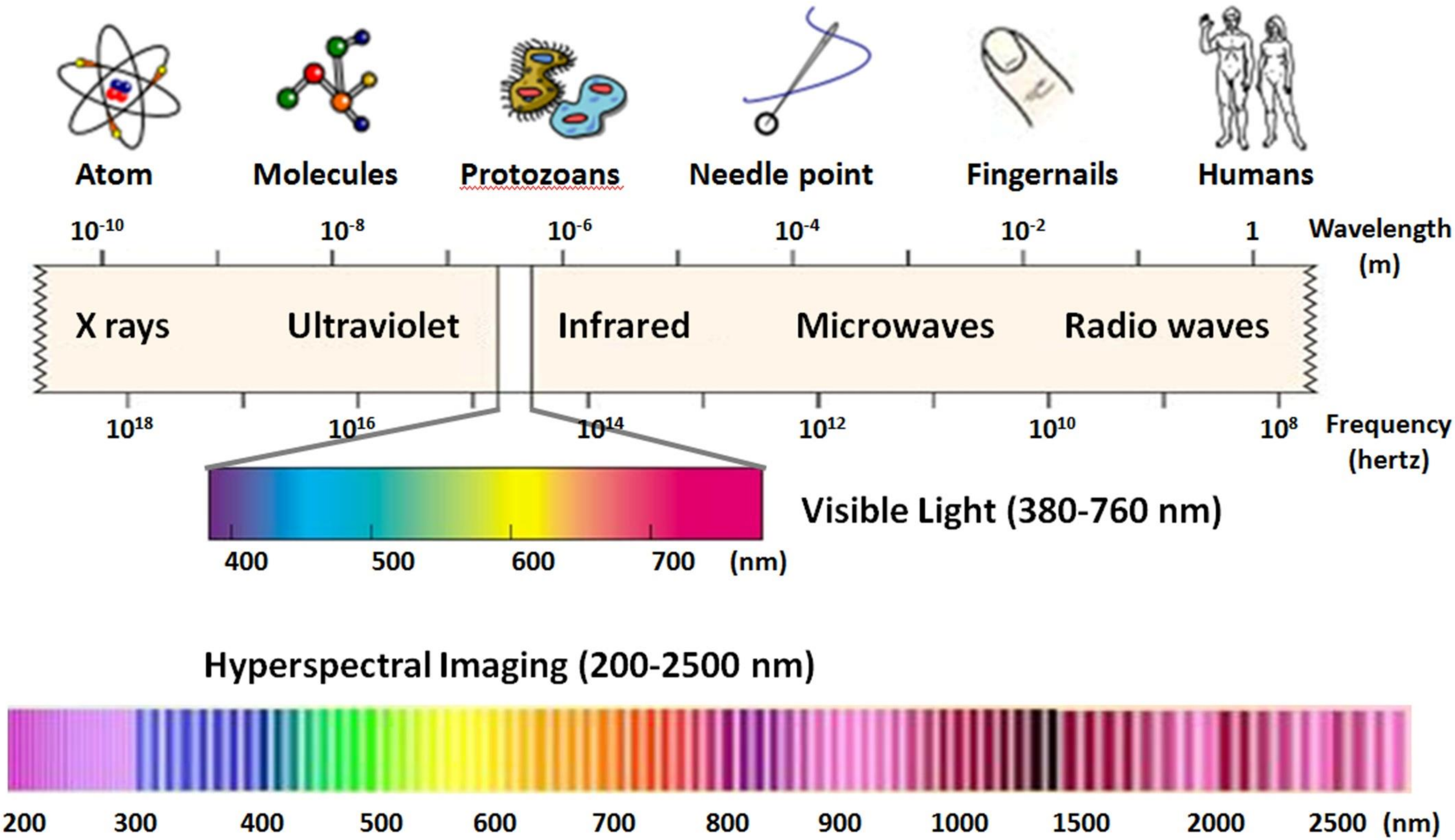

Opportunities & Challenges

- **High spatial resolution (*e.g.,* 5 μm)**
- **High spectral resolution (*e.g.,* 2 nm)**
- **Hundreds of spectral bands (*e.g.,* 650)**
- **Big data (*e.g.,* 5 GB per image)**
- **Quality control on data acquisition**
- **Lack of quantitative analysis tools**
- **Need high-performance computing power**
- **Need modeling and machine learning**

Applications of Hyperspectral Imaging

Cancer Detection

- Diagnosis of cancer *in vivo* and *ex vivo*

Image-guided Surgery

- Detection of residual tumor during surgery

Other Applications

- Detect diabetic foot
- Detect intestinal ischemia
- Measure tissue oxygen saturation
- Wound, nerves, dental, eye, blood vessel, and etc.

HSI Applications

Lu and Fei,
Medical hyperspectral imaging: a review. *J Biomed Opt*. 19(1):10901

Journal of Biomedical Optics

Top Downloads of 2018

Dear Baowei Fei,

These 18 papers had the most downloads in 2018. Now that the *Journal of Biomedical Optics* (JBO) is fully open access, all of these articles are freely available. Enjoy!

Brian W. Pogue
Dartmouth College
Editor-in-Chief

Most popular JBO downloads of 2018:

1. "Medical hyperspectral imaging: a review" by Guolan Lu and Baowei Fei

2. "Tutorial on photoacoustic tomography" by Yong Zhou, Junjie Yao, and Lihong V. Wang

3. "Optical properties of human skin" by Tom Lister, Philip A. Wright, and Paul H. Chappell

4. "Polarized light interaction with tissues" by Valery V. Tuchin

Table 1 Summary of representative hyperspectral imaging systems and their medical applications.

Reference	Spectral range (nm)	Spectral resolution (μm/pixel)	Detector	Dispersive device	Acquisition mode	Measurement mode	Application
14	400 to 1100	—	Si CCD	Filter wheel	Staring	Reflectance	Burn wounds
19	200 to 700	~5	CCD	Filter wheel	Staring	Fluorescence and reflectance	Cervical neoplasia
34	330 to 480	5	CCD	Filter wheel	Staring	Fluorescence and reflectance	Cervical cancer
35	530 to 680	12	CCD	Prism	Pushbroom	Transmission	Cutaneous wound
36	5000 to 10,526	11	HgCdTe	—	FTIR	Reflectance	Cervical pathology
37	500 to 600	—	CCD	LCTF	Staring	Reflectance	Diabetic foot
38	400 to 720	—	CCD	LCTF	Staring	Fluorescence	Tumor hypoxia and microvasculature
39	440 to 640	1 to 2	CCD; ICCD	AOTF	Staring	Fluorescence and reflectance	Skin cancer
40	500 to 600	—	CCD	LCTF	Staring	Reflectance	Hemorrhagic shock
41	365 to 800	~1	CCD	Prism	Pushbroom	Transmission	Melanoma
42 and 43	400 to 1000; 900 to 1700; 950 to 2500	5	Si CCD; InGaAs; HgCdTe	Grating	Pushbroom	Reflectance	Skin bruises
44	450 to 700	~1	FPA	CGH	Snapshot	Reflectance	Ophthalmology
45	450 to 700	—	CCD	LCTF	Staring	Reflectance	Breast cancer
46	650 to 1100	—	FPA	LCTF	Staring	Reflectance	Laparoscopic surgery
47	400 to 1000; 900 to 1700	5	CCD; InGaAs	PGP	Pushbroom	Reflectance	Intestinal ischemia
48	1000 to 2500	6.29	HgCdTe	PGP	Pushbroom	Reflectance	Gastric cancer
49	450 to 650	4 to 10	CCD	Prism	Snapshot	Reflectance	Endoscope
50	410 to 1000	—	Si CCD	Grating	Pushbroom	Reflectance and fluorescence	Atherosclerosis
51	400 to 720	—	CCD	LCTF	Staring	Reflectance	Diabetic foot
52	450 to 950	2	CCD	LCTF	Staring	Reflectance	Prostate cancer
53	390 to 680	—	CCD	Grating	Pushbroom	Reflectance	Laryngeal disorders
54	650 to 750	—	CCD	LCTF	Staring	Fluorescence and reflectance	Cholecystectomy
55	400 to 640	—	CCD	Filter wheel	Staring	Fluorescence and reflectance	Ovarian cancer
56	1000 to 2400	7	HgCdTe	LCTF	Staring	Reflectance	Pharmaceutical
57	900 to 1700	5	InGaAs	AOTF	Staring	Reflectance	Dental caries
58	550 to 950	2-5	CCD	AOTF	Staring	Transmission	Leucocyte pathology
59	550 to 1000	~2	CCD	AOTF	Staring	Transmission	Nerve fiber identification
60	2500 to 11,111	—	HgCdTe	—	FTIR	—	Breast cancer

Note: ICCD, intensified charge-coupled device; Si CCD, silicon CCD; LCTF, liquid crystal tunable filter; FPA, focal plane array; AOTF, acousto-optical tunable filter; CGH, computer-generated hologram; PGP, prism-grating-prism.

UT DALLAS The University of Texas at Dallas

UT Southwestern Medical Center

HSI for Cancer Detection

- **Molecular Level**
- **Cellular Level**
- **Tissue Level**
- **Physiological Level**

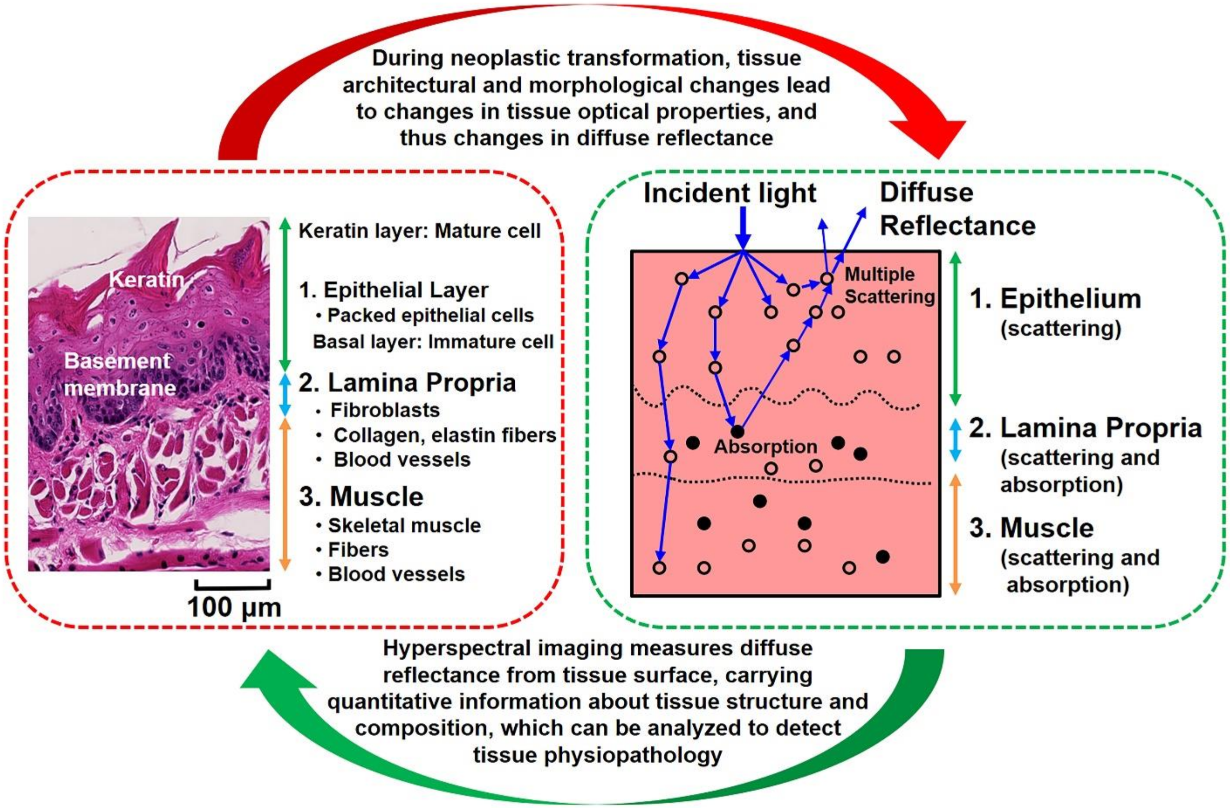

Lu, Wang, Qin, Muller, Little, Wang, Chen, Chen, and Fei.
Histopathology Feature Mining and Association with Hyperspectral Imaging for the Detection of Squamous Neoplasia. Nature Scientific Reports, 9(1), 17863

Spectral Signatures from HSI Data

Hypercube | **Average Spectra** | **Standard Deviations:**

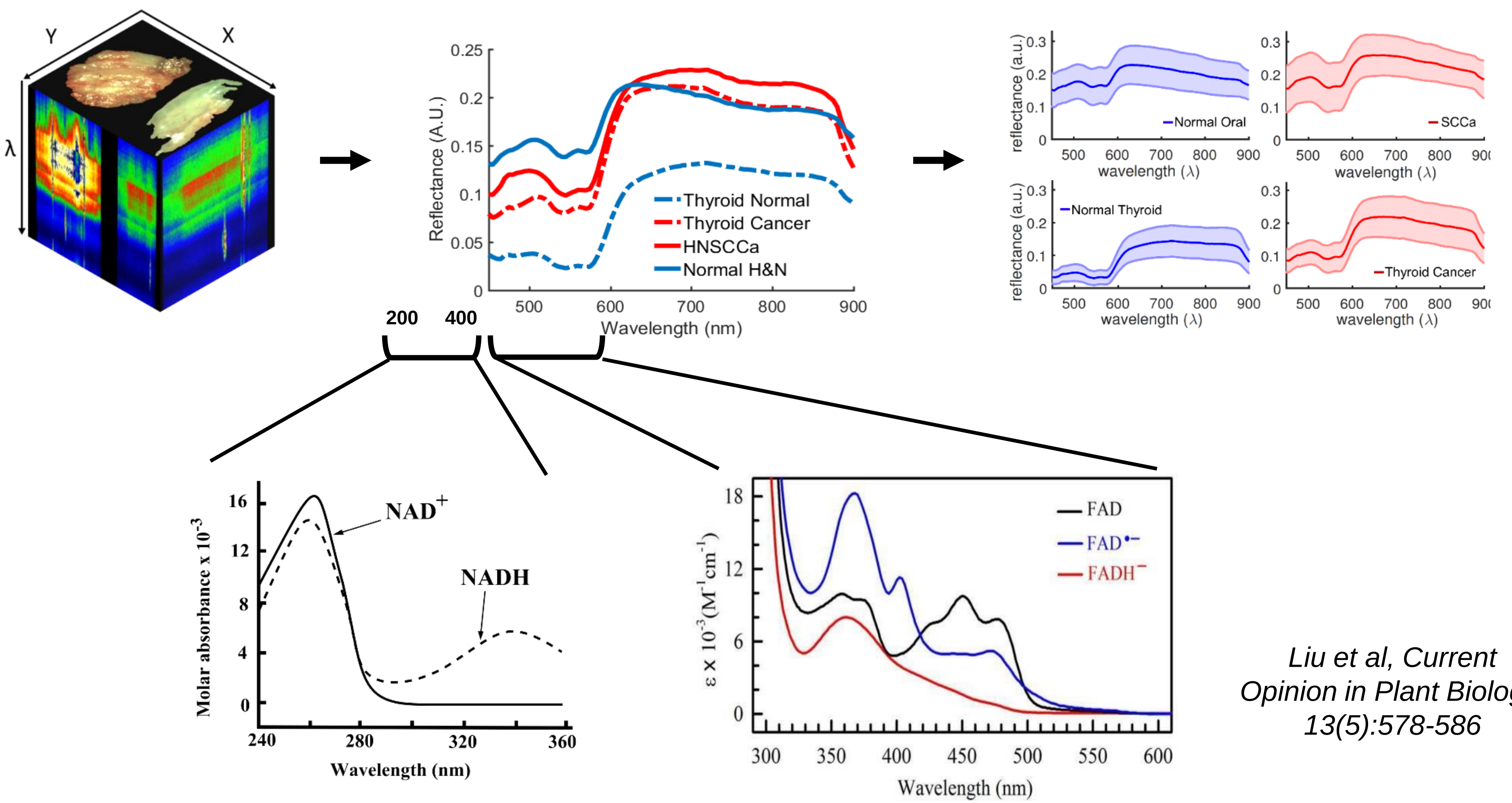

Liu et al, Current Opinion in Plant Biology. 13(5):578-586

UT DALLAS The University of Texas at Dallas

UTSouthwestern Medical Center

Spectral Signatures from HSI Data

Hypercube

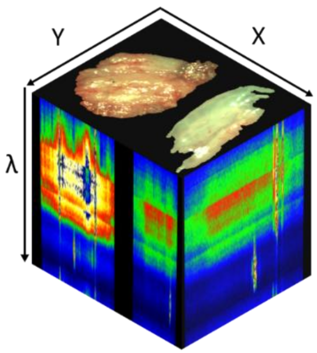

Average Spectra

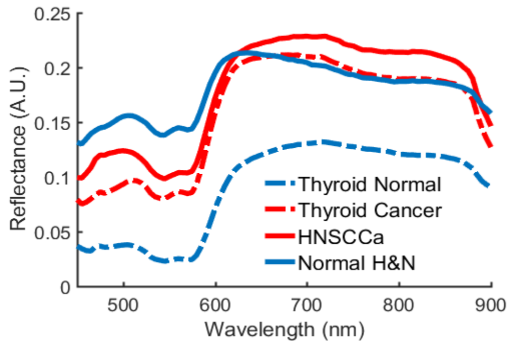

Standard Deviations:

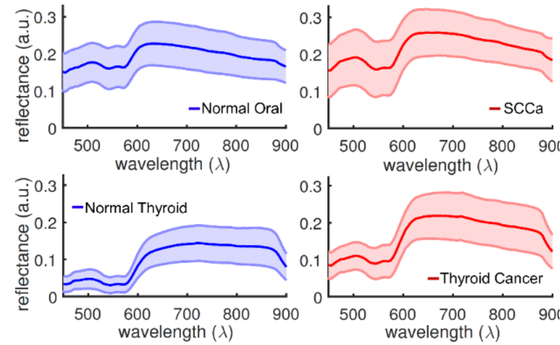

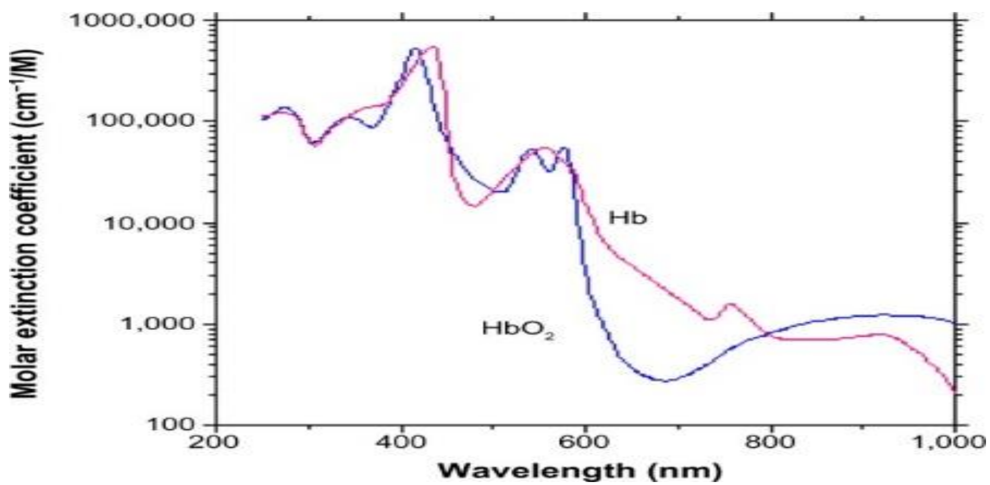

Nitzan et al, Med Devices. 2014;7:231-239

UT DALLAS
The University of Texas at Dallas

UTSouthwestern
Medical Center

Spectral Signatures from HSI Data

Hypercube

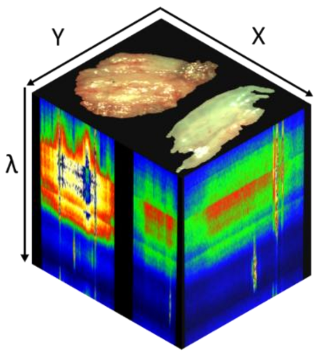

Average Spectra

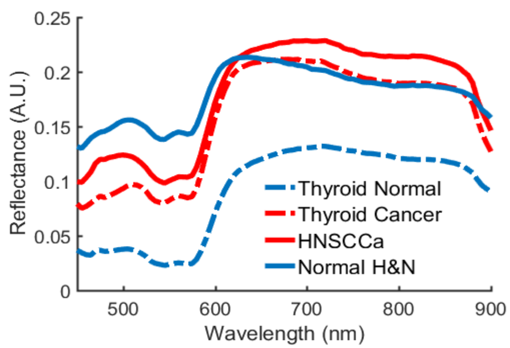

Standard Deviations:

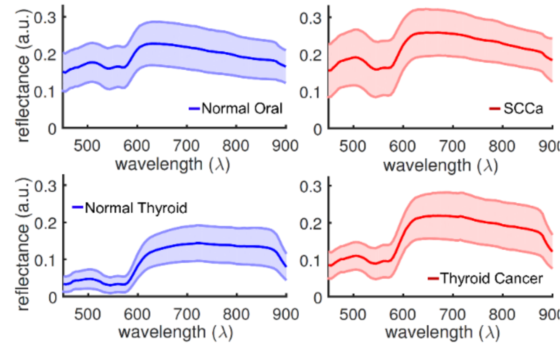

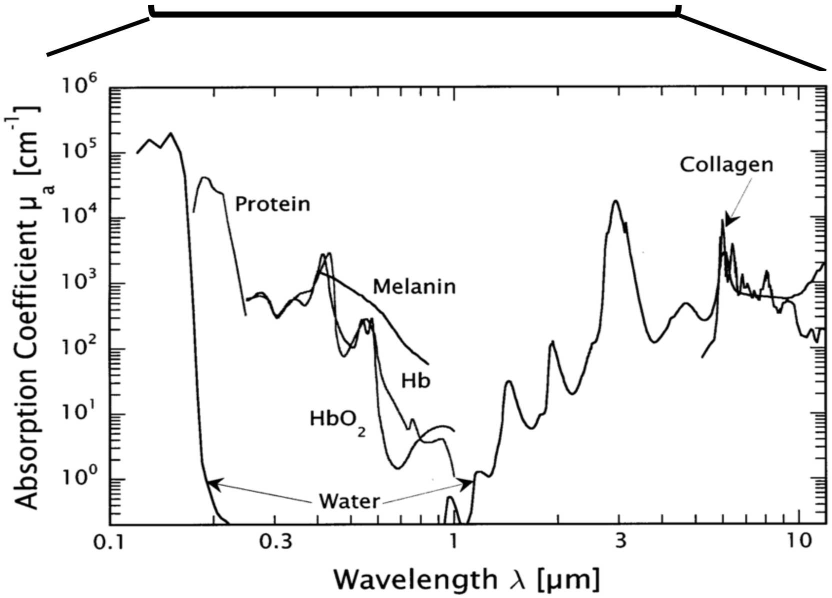

Vogel and Venugopalan, Chem. Rev. 103, 2, 577–644

UT DALLAS
The University of Texas at Dallas

UT Southwestern
Medical Center

Hyperspectral Imaging for Preclinical Studies

Head & Neck Cancer Detection in Animal Model

- Inject HNC cells with green fluorescence protein (GFP) into nude mice aged 4-6 weeks
- Acquire HSI image data
- Perform image quantification

Cancer Detection in Mice

889 | # 893 | # 894 | # 888

RGB

GFP

Probability Map

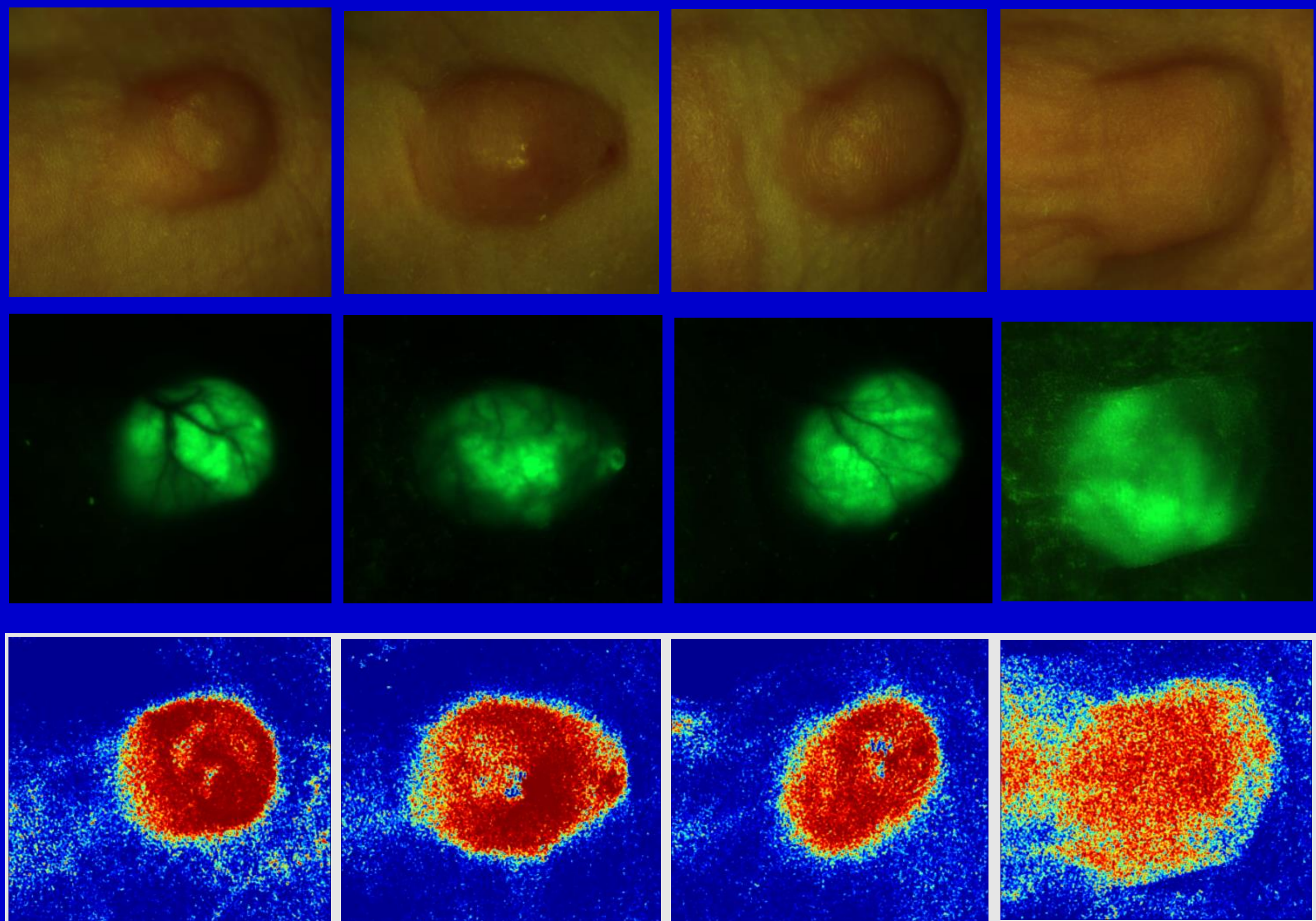

	# 889	# 893	# 894	# 888
Sensitivity	95%	96%	89%	84%

MSF-based Classification

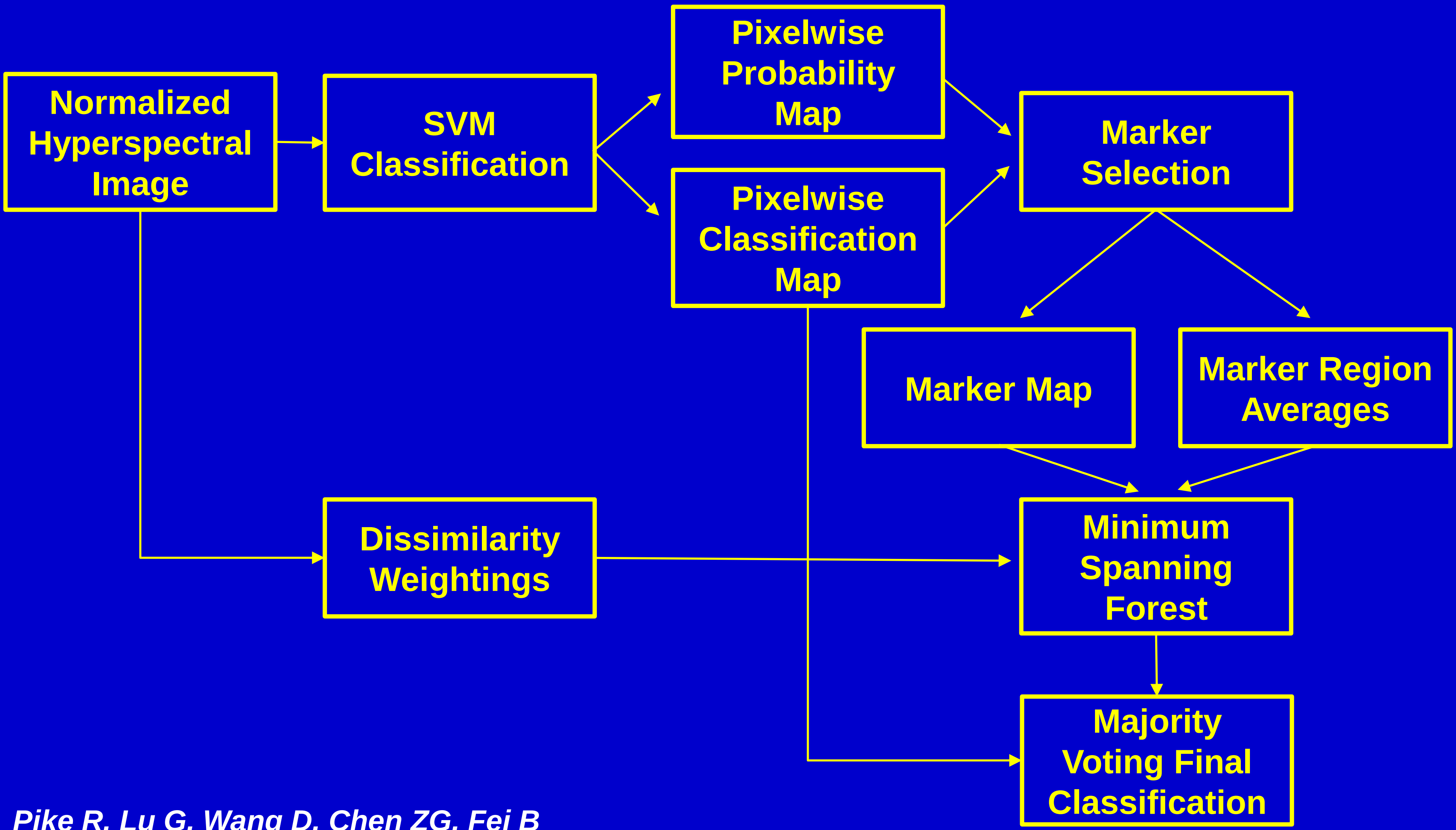

Pike R, Lu G, Wang D, Chen ZG, Fei B
IEEE Trans Biomed Eng. 63(3):653-63

Tensor-based Tissue Classification

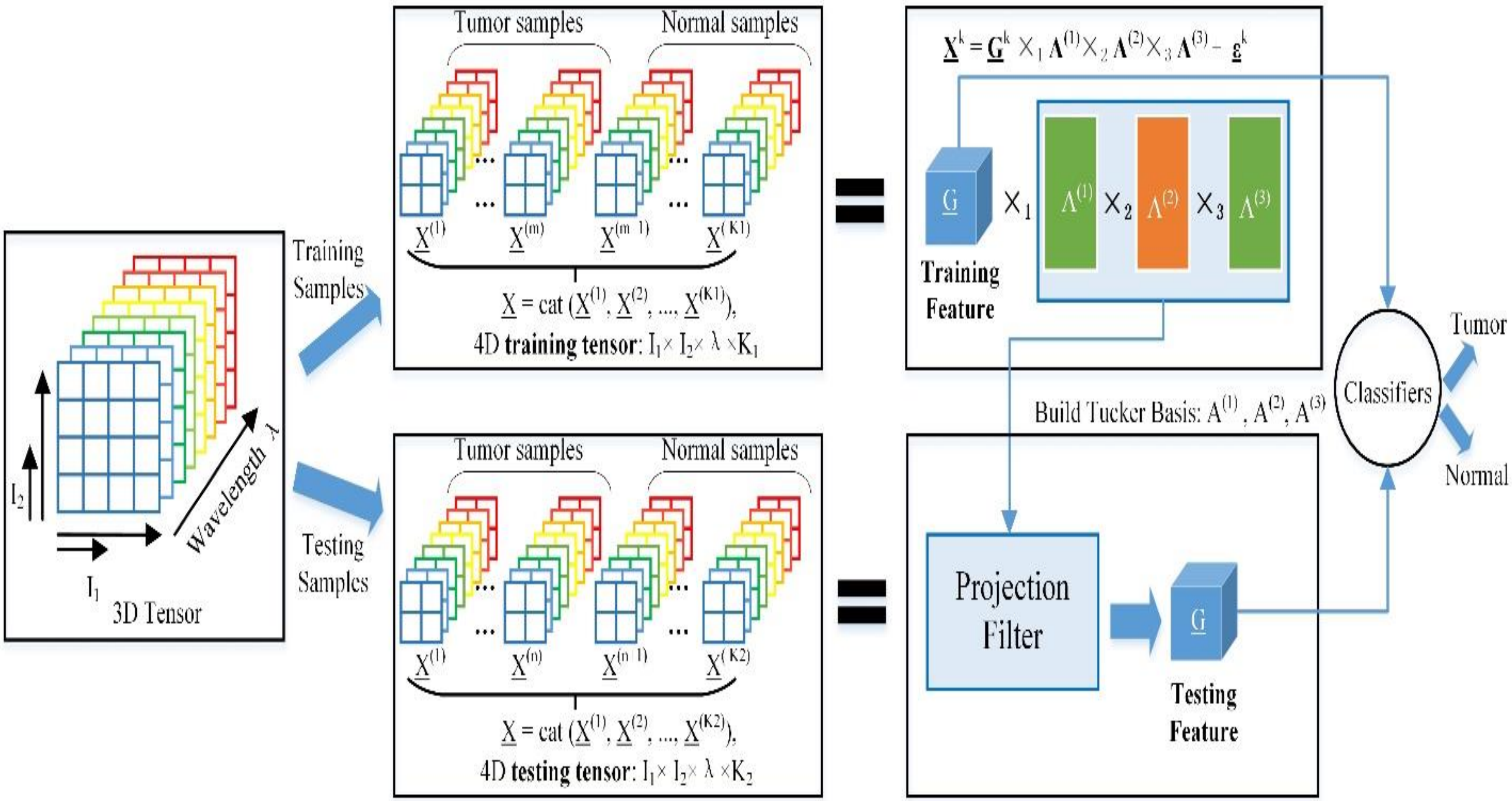

Lu G, Halig L, Wang D, Qin X, Chen ZG, Fei B,
J Biomed Opt. 19(10):106004

Comparison between Hyperspectral and Multispectral

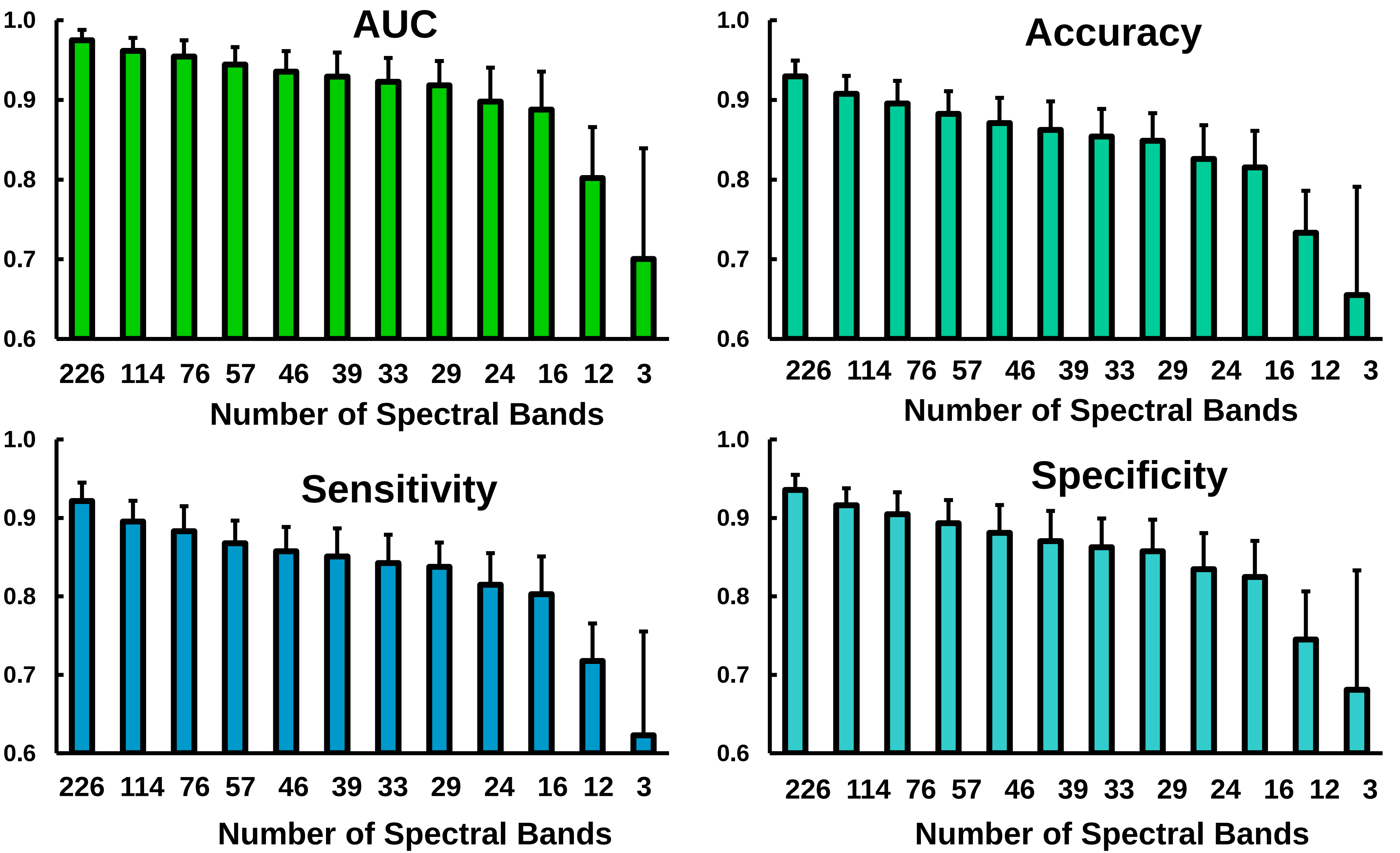

HSI for Head and Neck Cancer Detection in Chemically-induced Cancer Model

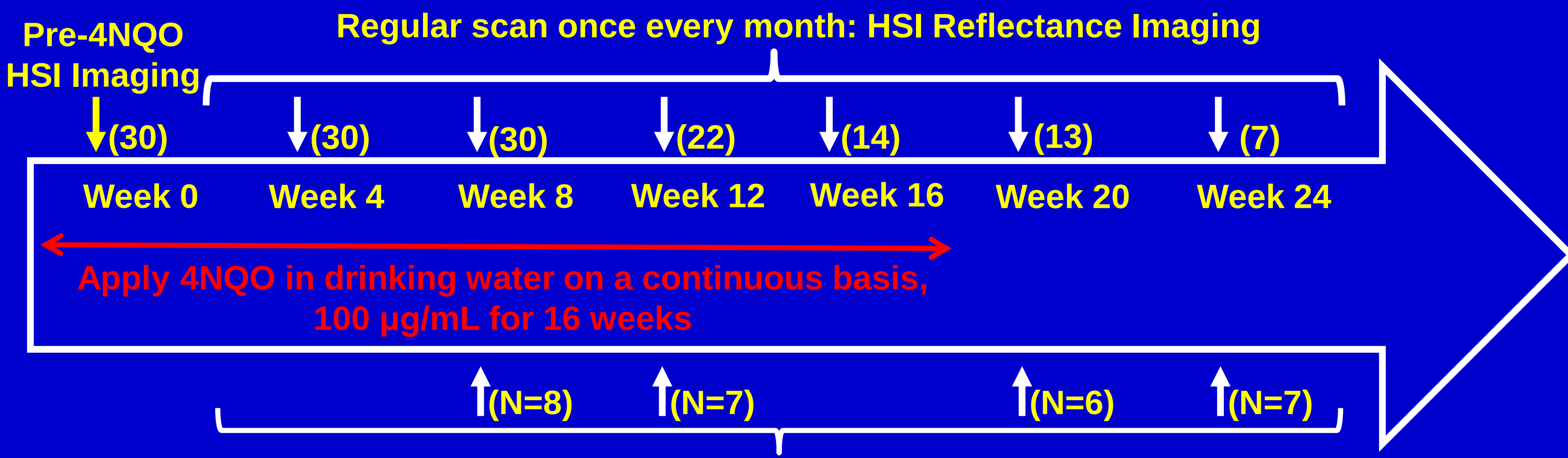

(1) White and Dark Reference
(2) *In vivo* reflectance imaging
(3) *In vivo* autofluorescence imaging
(4) Sacrifice N Mice and procure N Tongues

(5) *Ex vivo* reflectance imaging
(6) *Ex vivo* autofluorescence imaging
(7) *Ex vivo* 2-NBDG vital dye imaging
(8) *Ex vivo* proflavine vital dye imaging

4NQO: 4-nitroquinoline 1-oxide

Example Spectral Bands of Hypercube

450nm

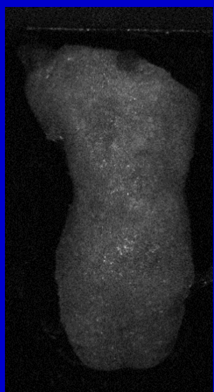

490nm

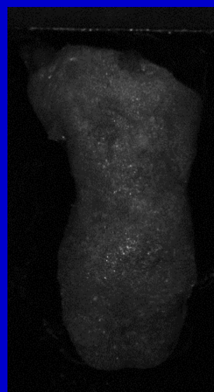

530nm

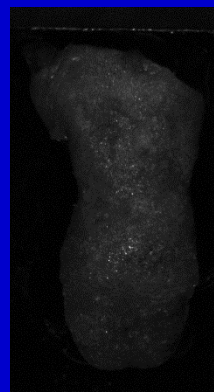

570nm

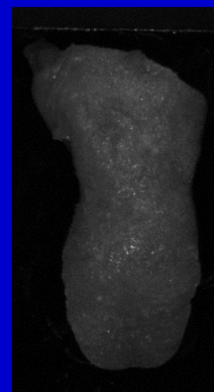

610nm

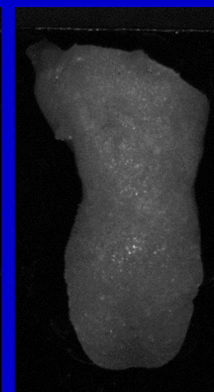

650nm

690nm

730nm

770nm

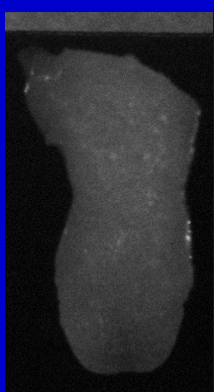

810nm

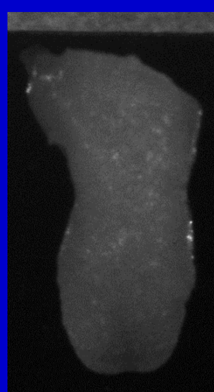

850nm

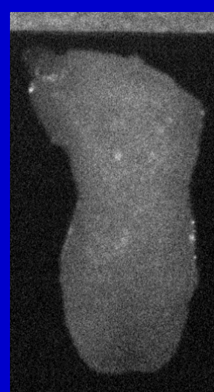

870nm

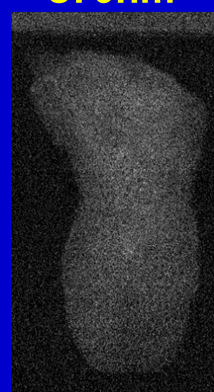

890nm

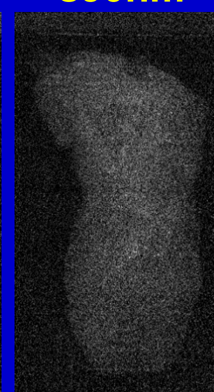

910nm

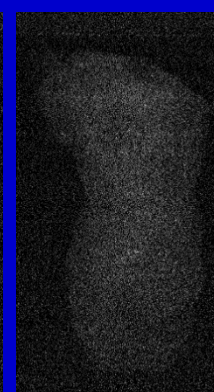

930nm

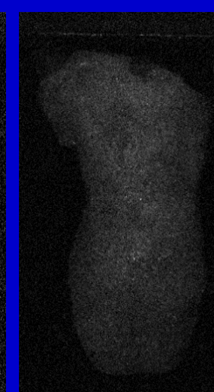

950nm

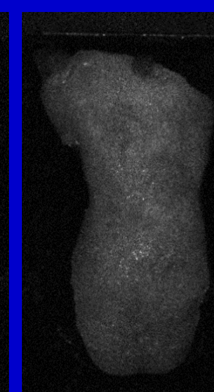

Reflectance Spectral Curve

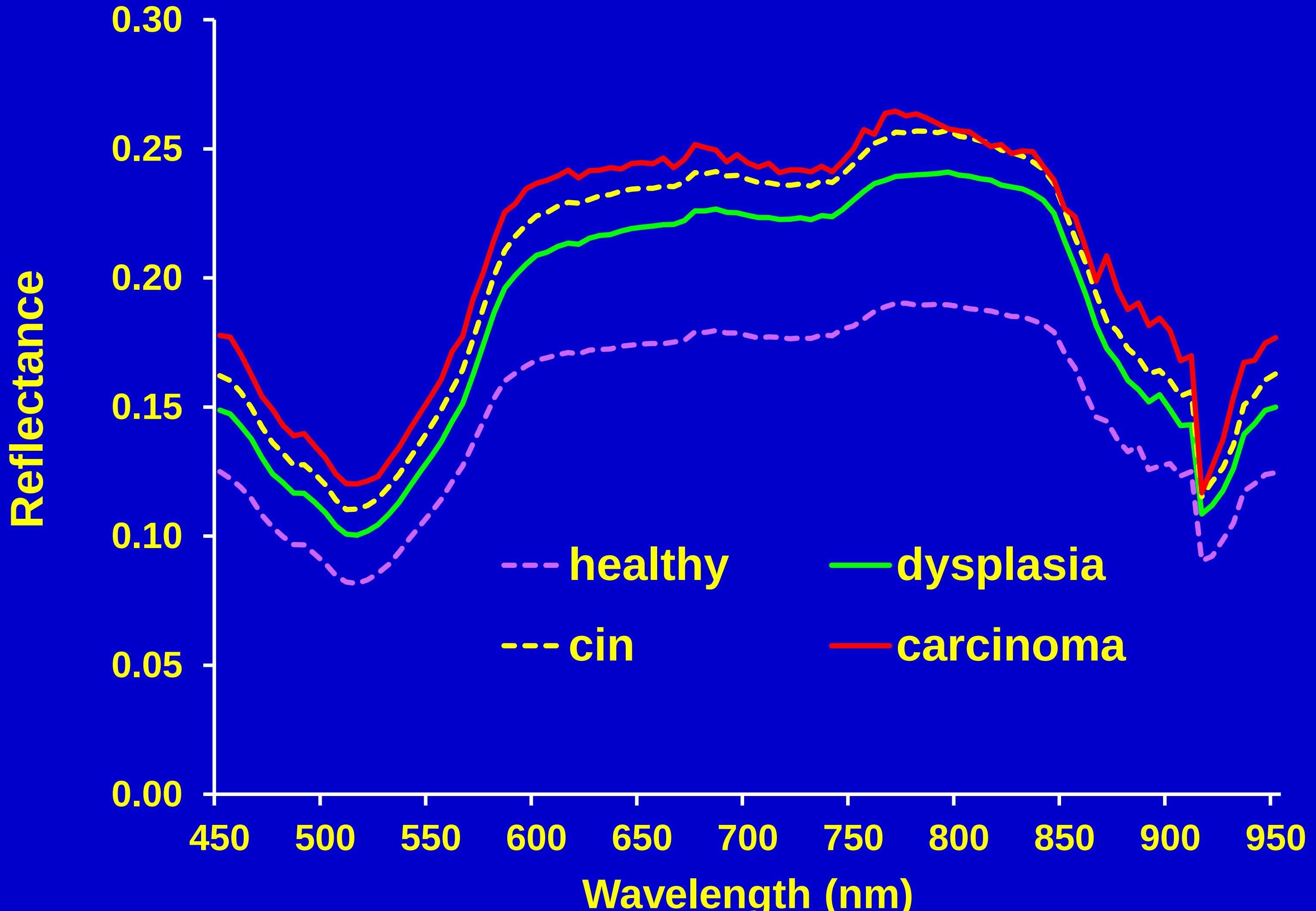

Histological Processing Procedure

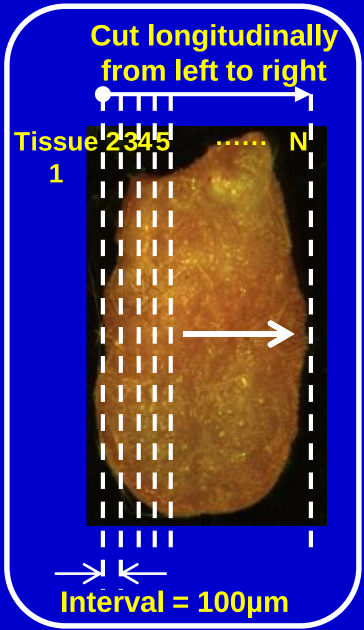

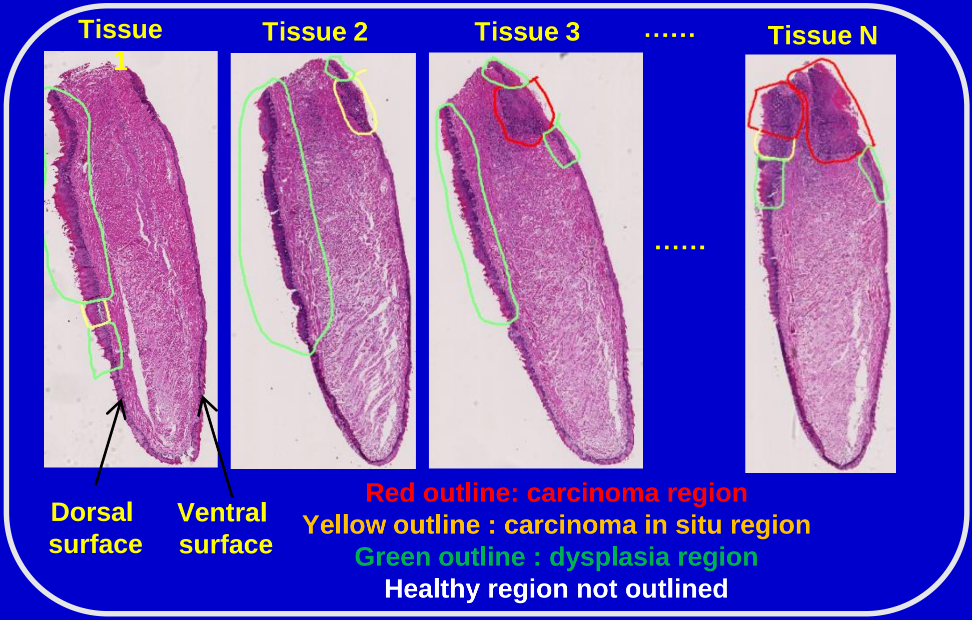

Ex Vivo Tongue

Histological Slides of the Tongue

Pathology Grading

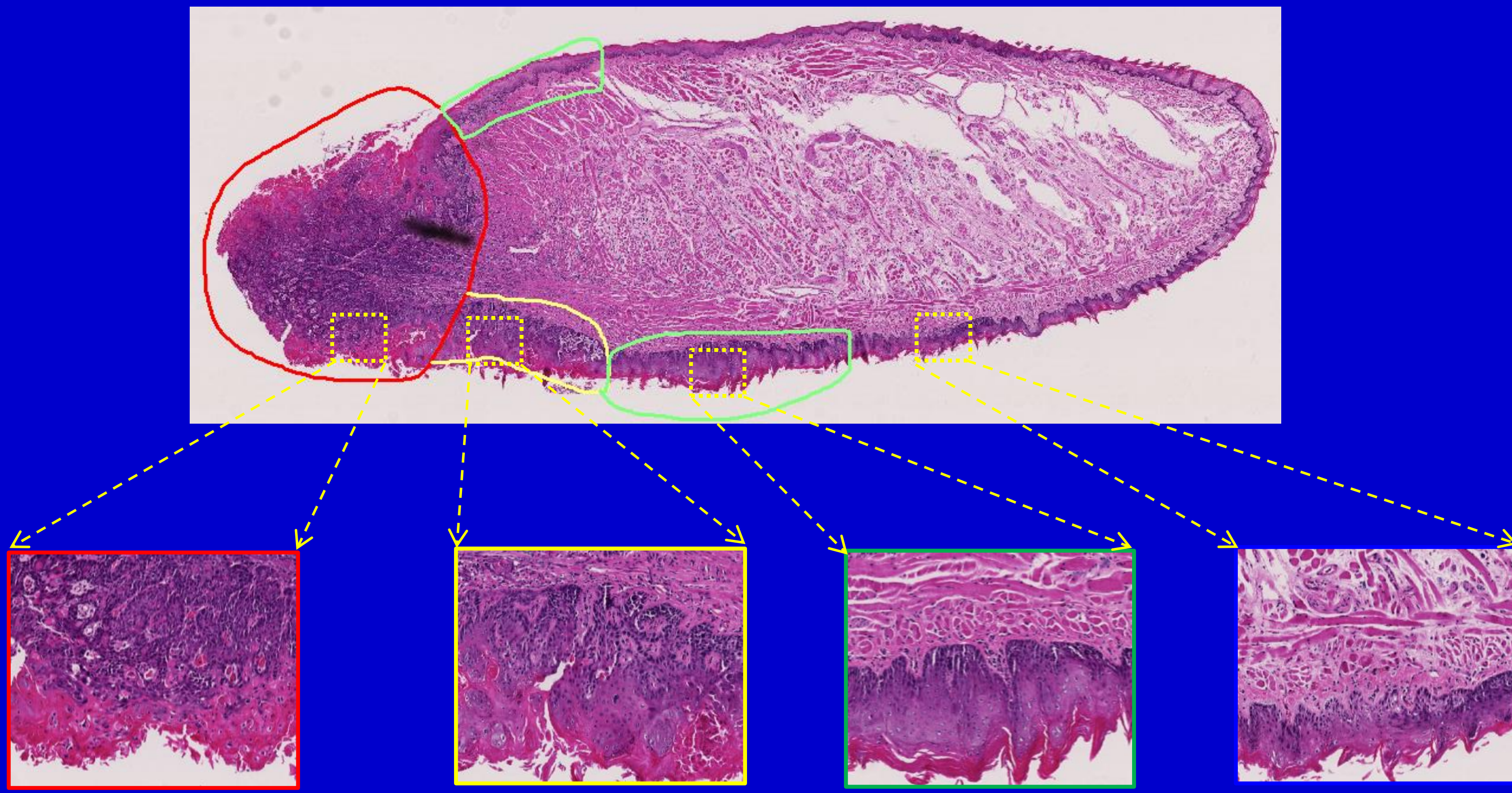

Carcinoma | Carcinoma in situ | Dysplasia | Healthy tissue

Outlined by Dr. Susan Muller, Head and Neck Pathologist

Histological Validation

Pathology Slides

Red: carcinoma;
Yellow: CIN;
Green: dysplasia

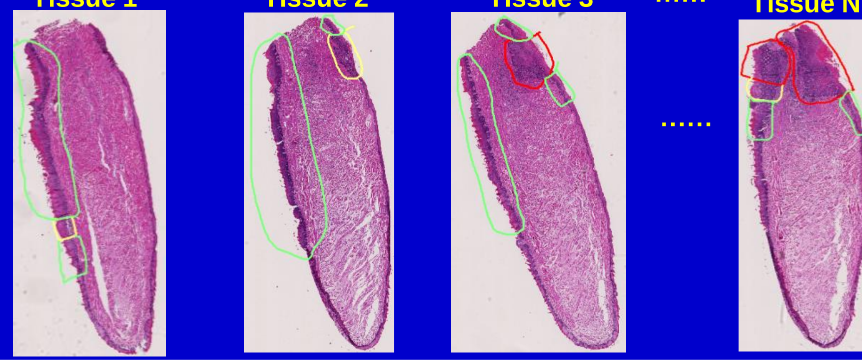

***Ex Vivo* Tongue**
Gold standard map

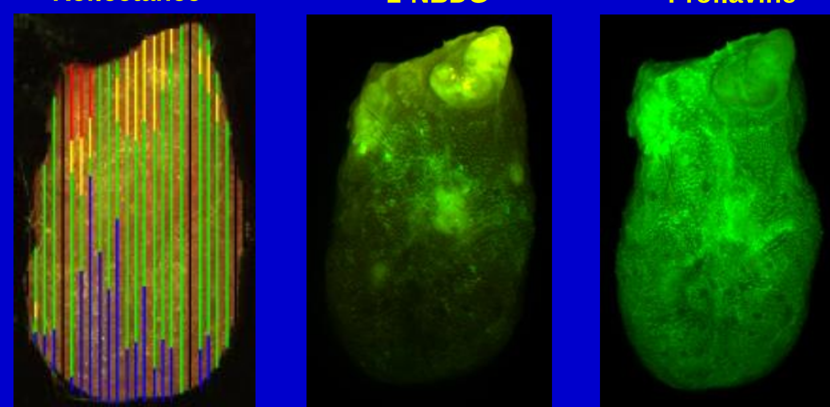

Classification Methods for HSI

- **11 Classifiers:**
  - Linear Discriminate Analysis (LDA)
  - Quadratic Discriminant Analysis (QDA)
  - K-Nearest Neighbors (KNN)
  - Naïve Bayes
  - Support Vector Machine (SVM)
  - Random Forest (RF)
  - Ensemble LDA
  - Ensemble KNN
  - Adaboost
  - RUSboost
  - RobustBoost
- **Performance metrics:**
  - ROC, AUC, Accuracy, Sensitivity, Specificity, NPV, PPV

Diagnostic Accuracy of Hyperspectral Imaging with Different Classifiers

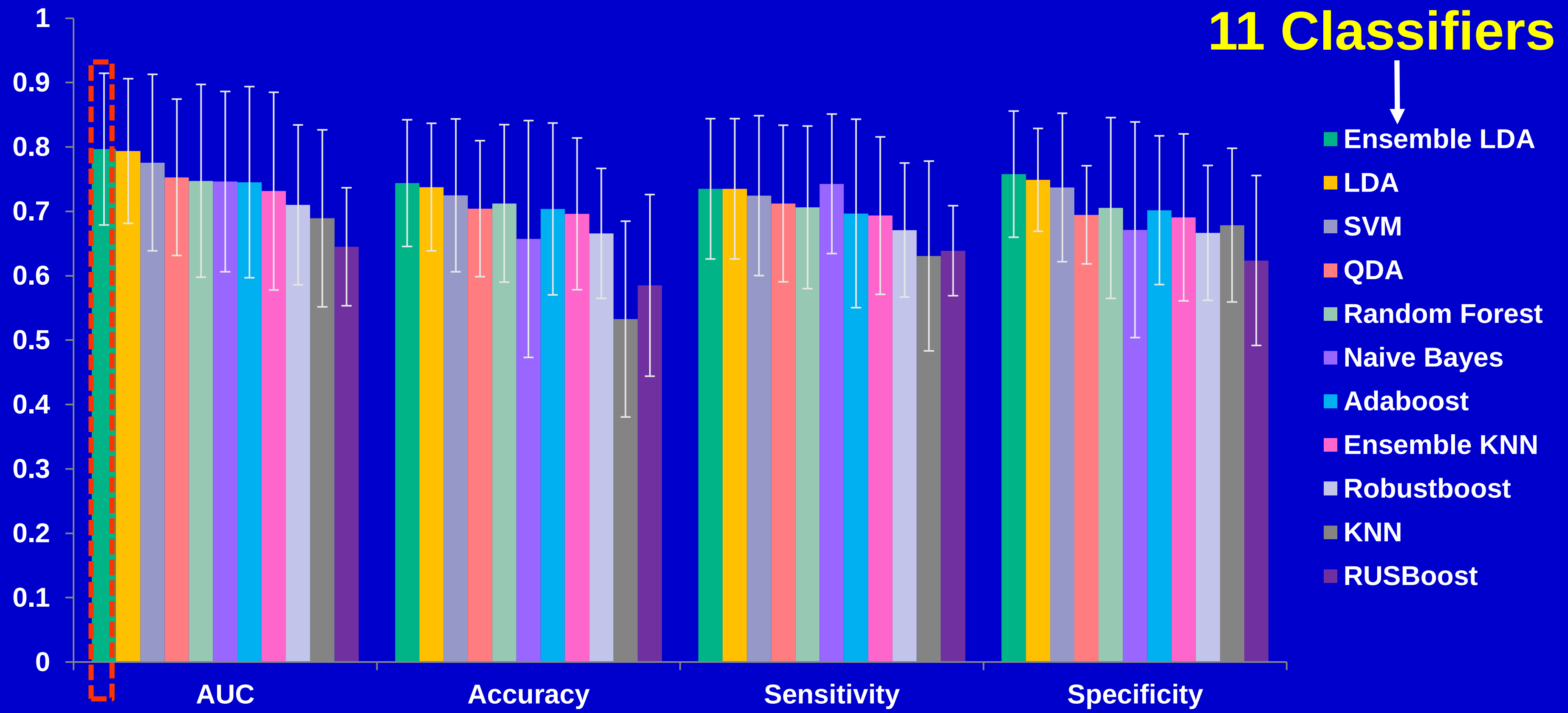

Ensemble LDA > LDA >SVM

AUC 0.797 0.794 0.776

Hyperspectral Imaging for Clinical Studies

Clinical Study of 204 Human Patients

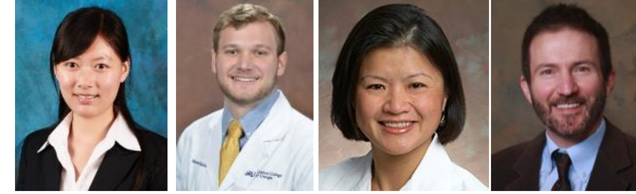

Patient Recruitment	Tissue Specimens	Hyperspectral Imaging	Histology Ground Truth

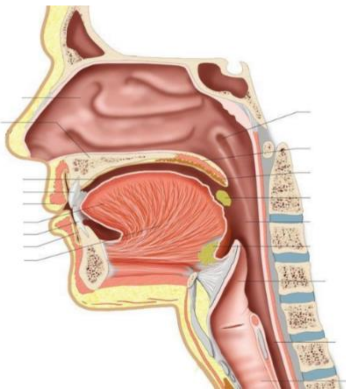

Head & Neck Cancer
***N* = 204 Patients**

Normal

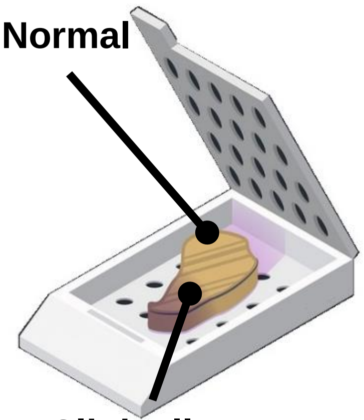

Clinically Visible Tumor

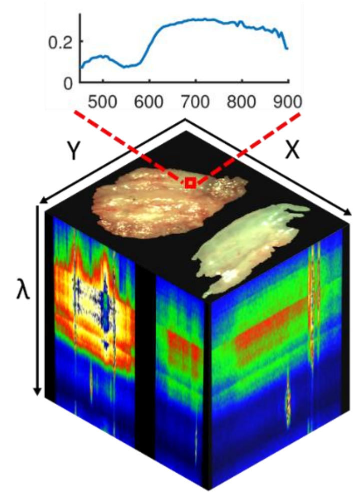

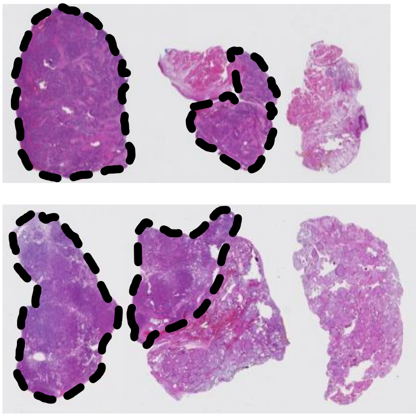

Certified Pathologist Outlined Cancer

***N* = 204**

3 per pt. *N* = 585

Fei et al. Journal Biomedical Optics 22(8):086009

Lu et al. Clinical Cancer Research. 23(18):5426-5436

Halicek et al. Biomedical Optical Express. 11(3):1383-1400

Halicek et al. Cancers;1(9):1367

UT DALLAS The University of Texas at Dallas

UT Southwestern Medical Center

H&N Cancer Patient Population

HNSCC		Thyroid	
SCC, Conventional	85	Thyroid, Papillary	54
SCC, HPV+ (p16+)	13	Thyroid, Follicular	13
SCC, Basaloid	1	Thyroid, Medullary	5
SCC, Neuroendocrine	1	Thyroid, Insular	1
SCC, Spindle Cell	1	Thyroid, Poorly Diff. Ca	3
Adenosquamous Carcinoma	1	Thyroid, Benign Goiter	6
Total	**102**	**Total**	**82**

Other (Not used)		Salivary Glands	
Spindle Cell Carcinoma	1	Pleomorphic Adenoma	2
Osteosarcoma	1	Mucoepidermoid Carcinoma	1
Reactive Tonsil	1	Salivary Duct Carcinoma	1
Lymph Nodes	1	Polymorphous LG Adenoma	1
Lung Adenocarcinoma	1	Adenoid Cystic Carcinoma	1
Jugular Vein SCC Metastasis	1	**Total**	**6**
Incomplete Information	8		
Total	**14**		

UT DALLAS The University of Texas at Dallas

UTSouthwestern Medical Center

HSI Database of Tissue Specimens

- **567 specimens from 204 patients**
- **43 million pixels of spectral data**
- **Normal (N): 196 Tissues**
  - **11,590,587 pixels of spectra**
- **Tumor (T): 141 Tissues**
  - **10,343,782 pixels of spectra**
- **TN Margin: 230 Tissues**
  - **N pixels: 9,721,168**
  - **T pixels: 11,307,392**

Spectra of Different Tissues

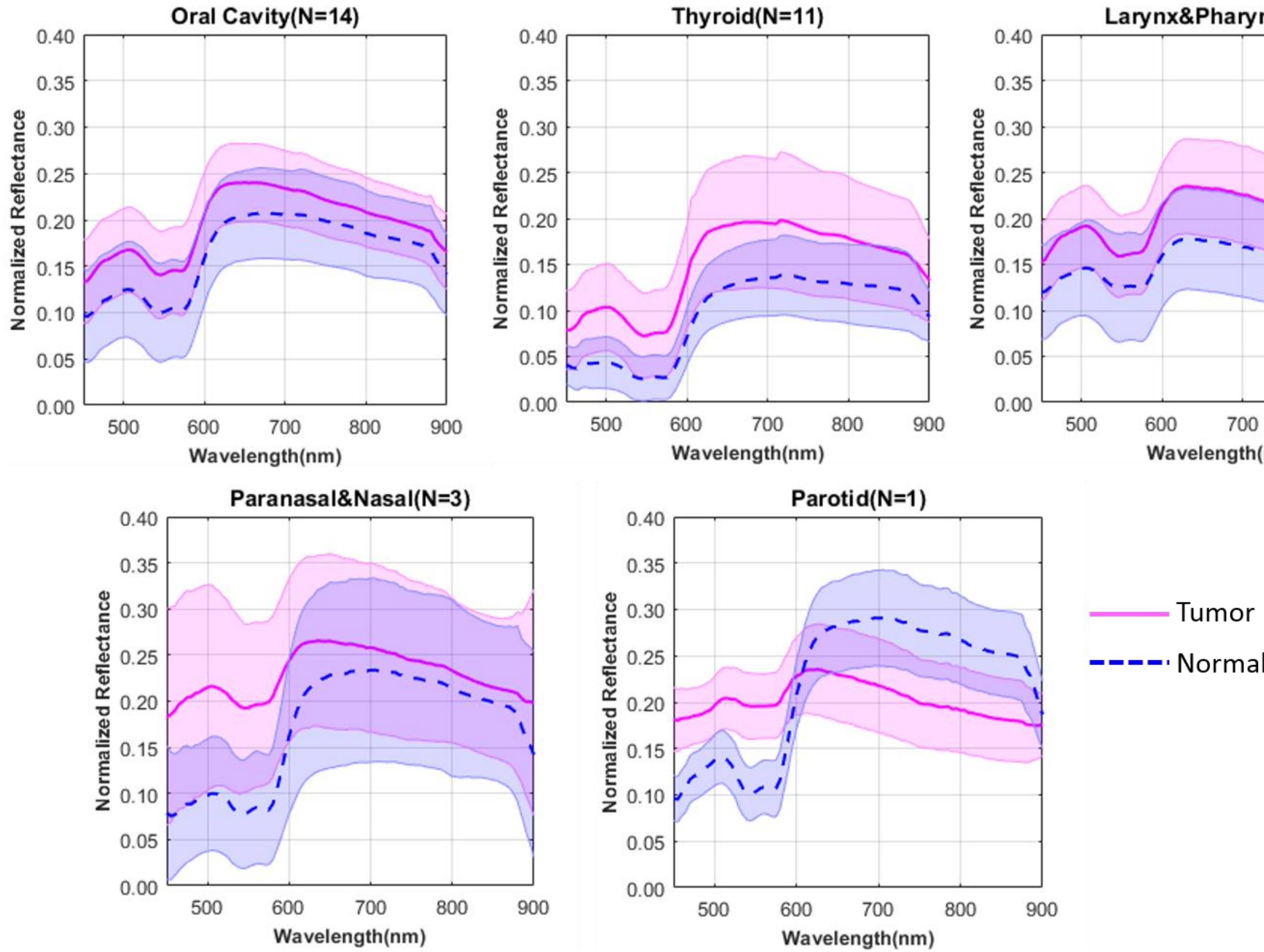

HSI Data Processing Framework

Hypercube → **Pre-processing** → **Feature Extraction** → **Feature Selection and Classification**

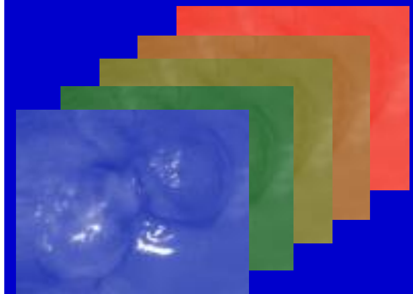

Pre-processing:

- Data Normalization
- Image Registration
- Glare Detection and Removal
- Curvature Correction

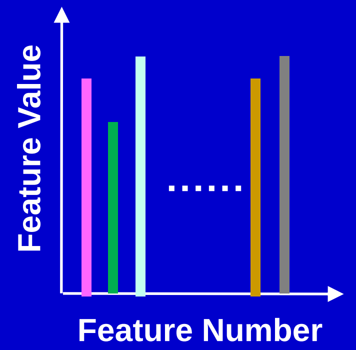

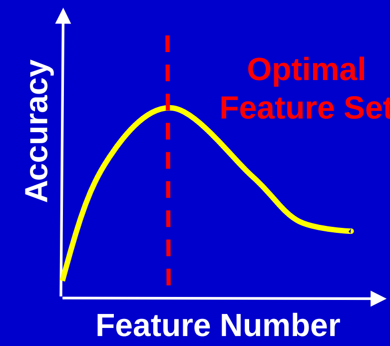

Feature Selection with Leave-One-Out Cross Validation

Data Partition → **Feature Extraction** → **Feature Selection (m)** → **Classification** → **Prediction**

Vary Feature Number (m) to Be Selected

Tumor Margin Assessment of Fresh Surgical Tissue Specimens of Human Patients

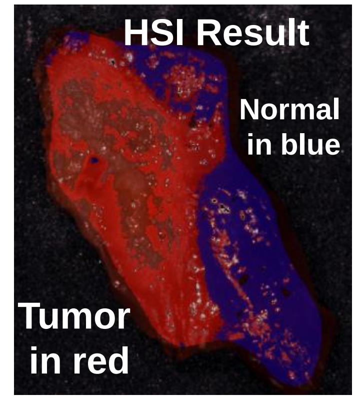

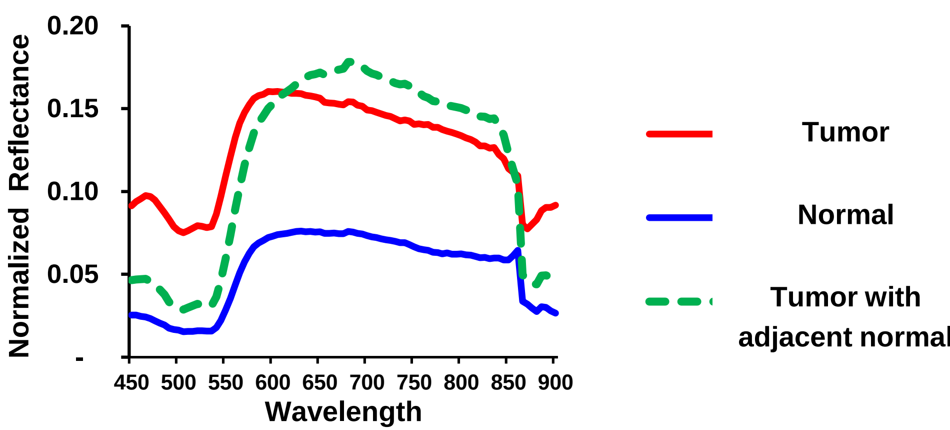

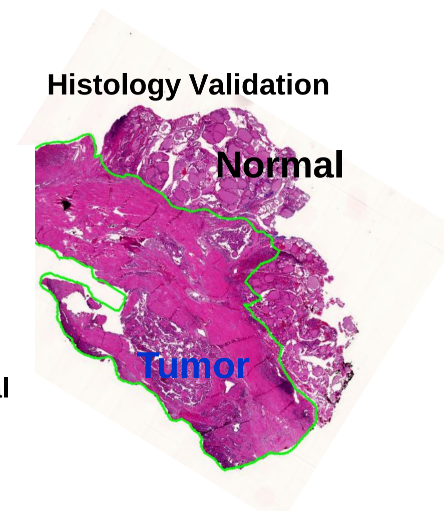

Fei et al. Journal Biomedical Optics 22(8):086009

UT DALLAS The University of Texas at Dallas

UTSouthwestern Medical Center

Conventional Machine Learning Methods for Tumor Mapping on HSI Data

- **Support vector machines (SVM)**
- **Linear discriminant analysis (LDA)**
- **Quadratic discriminant analysis (QDA)**
- **SVMs with RBF Kernel**
- **Random Forest**
- **Ensemble LDA**
- **RUSBoost**

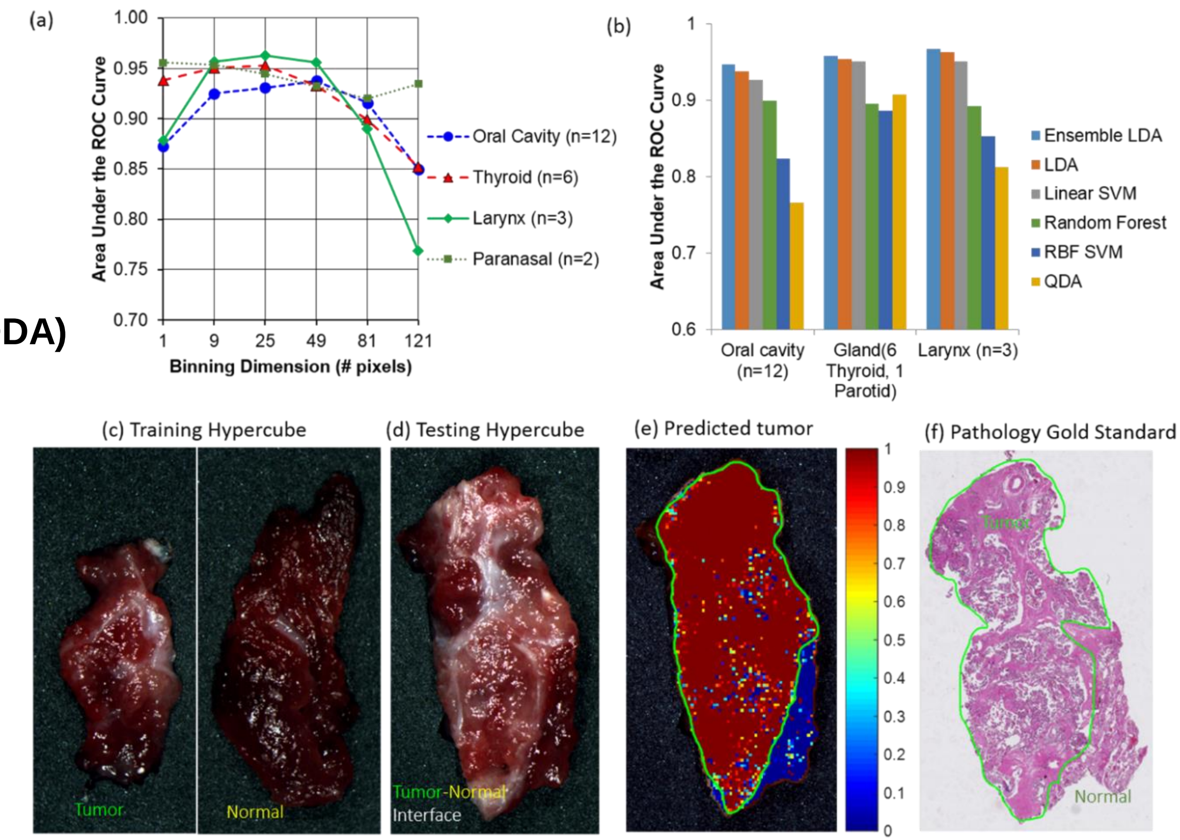

Lu G, Little JV, Wang X, Zhang H, Patel MR, Griffith CC, El-Deiry MW, Chen AY, Fei B. Clinical Cancer Research. 23(18):5426-5436

UT DALLAS The University of Texas at Dallas

UTSouthwestern Medical Center

Representative Prediction Results
(Tongue Squamous Cell Carcinoma)

Training Hypercube

Tumor Normal

Testing Hypercube

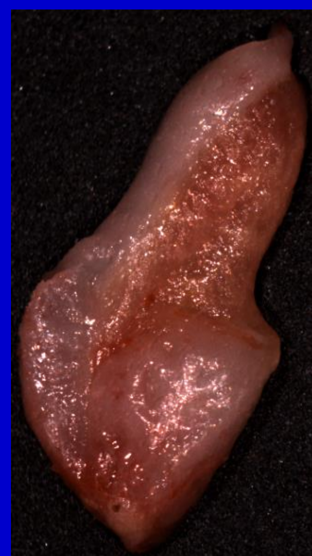

Tumor-Normal Interface

Predicted tumor map

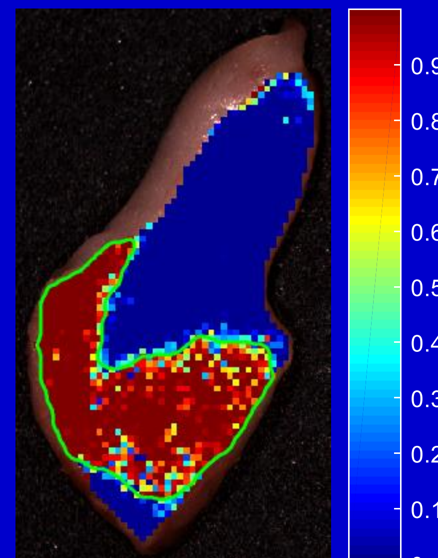

Pathology Gold Standard

Help surgeons to assess the tumor border during surgery

Conventional Machine Learning *vs.* Deep Learning

Conventional Machine Learning

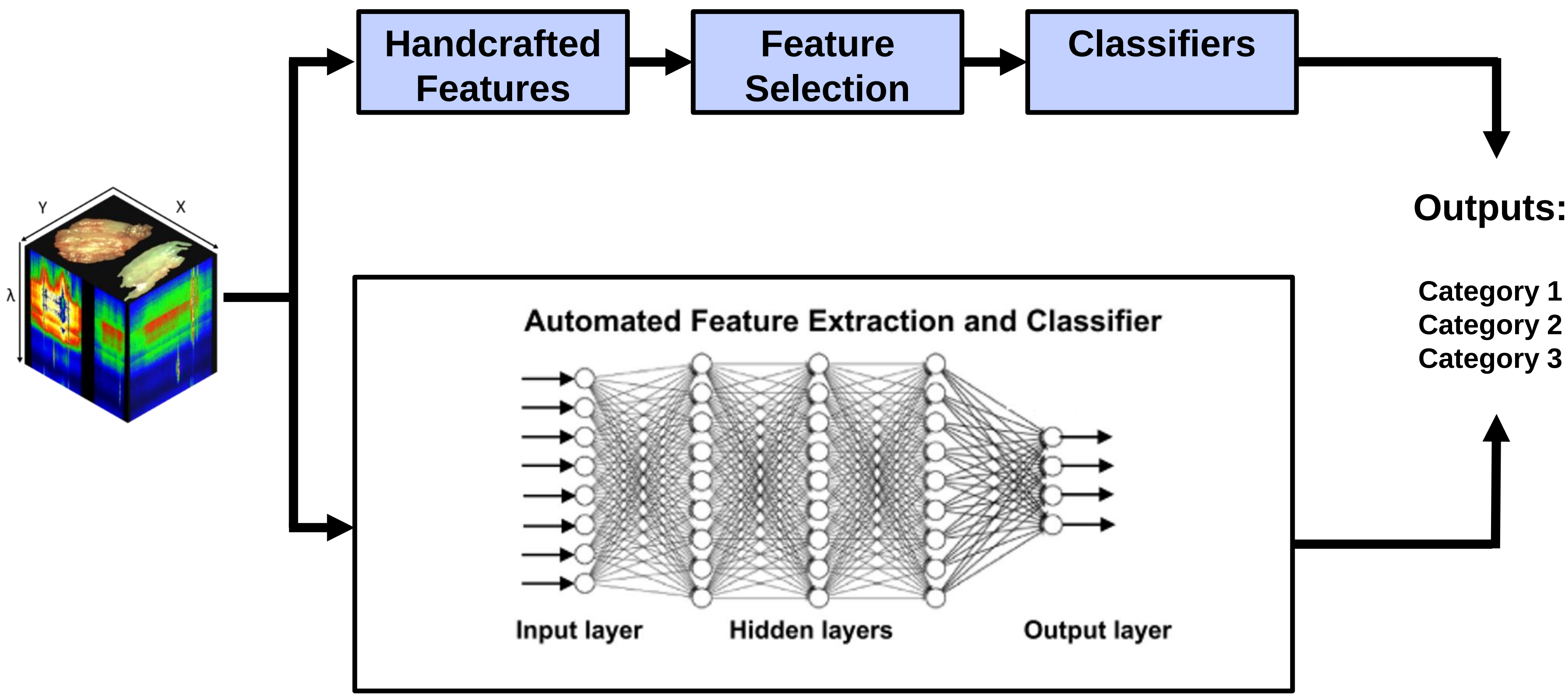

Deep Learning

UT DALLAS The University of Texas at Dallas

UT Southwestern Medical Center

Convolutional Neural Networks (CNN) for Detection of Squamous Cell Carcinoma (SCC)

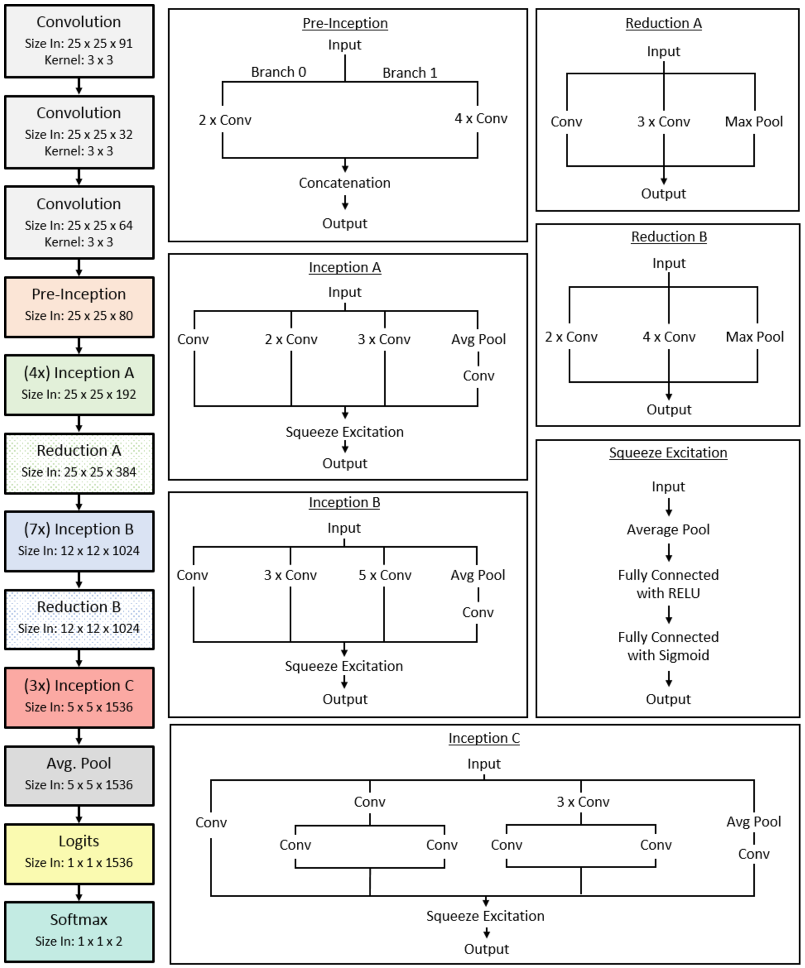

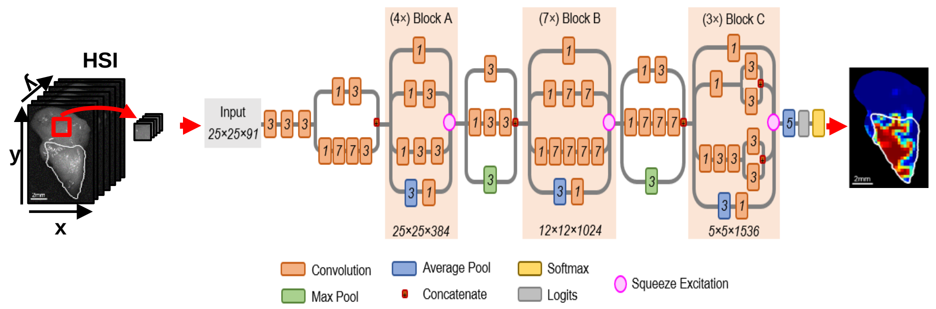

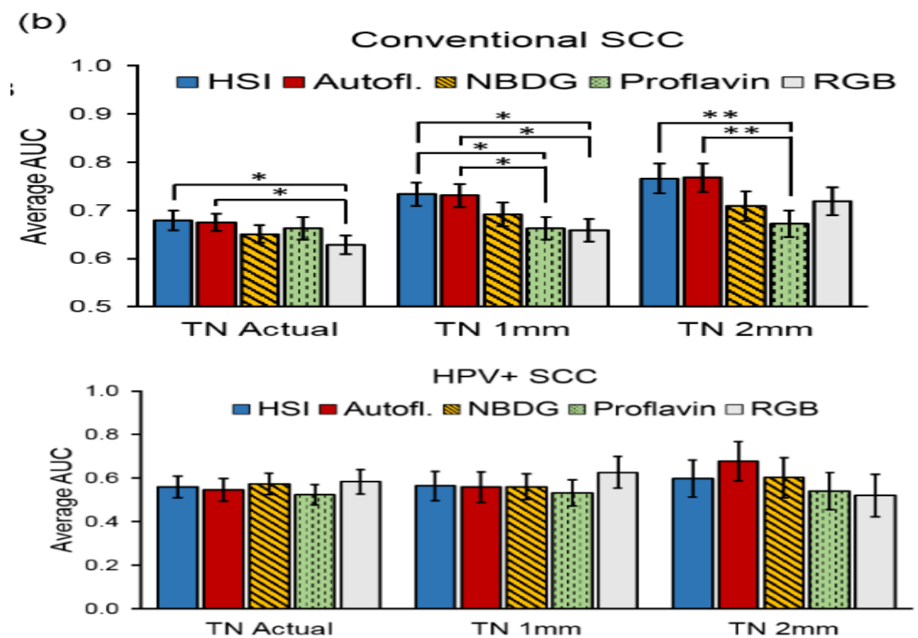

Halicek M, Dormer JD, Little JV, Chen AY, Myers L, Sumer BD, Fei B. Hyperspectral Imaging of Head and Neck Squamous Cell Carcinoma for Cancer Margin Detection in Surgical Specimens from 102 Patients Using Deep Learning. Cancers. 11(9):1367.

UT DALLAS
The University of Texas at Dallas

UTSouthwestern
Medical Center

CNN for Thyroid Tumor Detection

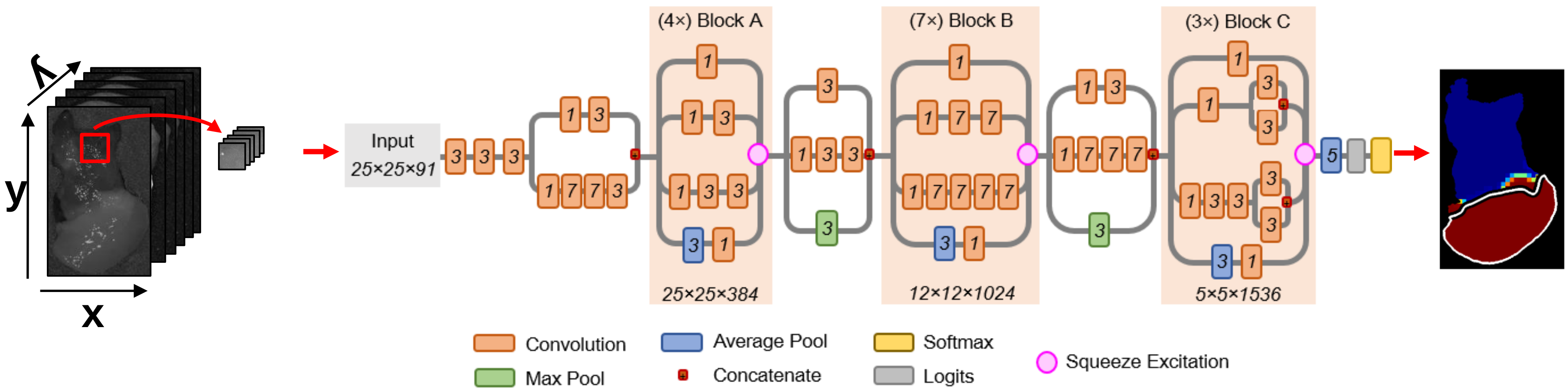

- Loss function: cross-entropy
- Optimizer: Adadelta
- Initial learning rate: 1.0
- Augmentation: 8 x
- Training: 23 hrs
- Testing: 20 ± 8 sec with a single GPU

Pt. 01 – 15	Fold 1	Training & Validation	...	Testing
Pt. 16 – 30	Fold 2			Training & Validation
Pt. 31 – 45	Fold 3			
Pt. 46 – 60	Fold 4			
Pt. 61 – 76	Fold 5	Testing		

		AUC	Accuracy	Sensitivity	Specificity
HSI	Combined	0.86 ± 0.02	78 ± 2%	80 ± 3%	74 ± 3%
	PTC	0.86 ± 0.02	76 ± 2%	79 ± 3%	71 ± 4%
	MTC & Insular Ca.	0.81 ± 0.09	85 ± 5%	85 ± 5%	72 ± 11%
	Follicular Ad/Ca.	0.90 ± 0.04	80 ± 4%	80 ± 7%	82 ± 5%
	Poorly Diff. Ca.	0.90 ± 0.08	81 ± 15%	73 ± 23%	96 ± 4%
Autofluorescence	Combined	0.85 ± 0.02	76 ± 2%	83 ± 2%	68 ± 3%
	PTC	0.81 ± 0.03	72 ± 2%	79 ± 3%	62 ± 4%
	MTC & Insular Ca.	0.86 ± 0.06	80 ± 5%	83 ± 7%	78 ± 6%
	Follicular Ad/Ca.	0.95 ± 0.02	87 ± 3%	93 ± 3%	81 ± 5%
	Poorly Diff. Ca.	0.98 ± 0.01	95 ± 1%	95 ± 3%	93 ± 1%
HSI-synthesized Gaussian-RGB	Combined	0.89 ± 0.02	79 ± 2%	77 ± 2%	82 ± 3%
	PTC	0.87 ± 0.02	77 ± 2%	76 ± 3%	79 ± 4%
	MTC & Insular Ca.	0.95 ± 0.03	88 ± 4%	91 ± 4%	82 ± 8%
	Follicular Ad/Ca.	0.90 ± 0.02	77 ± 3%	67 ± 6%	91 ± 2%
	Poorly Diff. Ca.	0.98 ± 0.01	94 ± 3%	92 ± 4%	95 ± 4%
HSI-synthesized Human-Eye RGB	Combined	**0.90 ± 0.02**	**79 ± 2%**	**80 ± 2%**	**79 ± 3%**
	PTC	0.88 ± 0.02	78 ± 2%	80 ± 3%	76 ± 4%
	MTC & Insular Ca.	0.96 ± 0.02	88 ± 3%	93 ± 3%	85 ± 6%
	Follicular Ad/Ca.	0.92 ± 0.02	76 ± 3%	68 ± 7%	86 ± 4%
	Poorly Diff. Ca.	0.99 ± 0.01	91 ± 3%	92 ± 3%	93 ± 5%

Halicek M, Dormer JD, Little JV, Chen AY, Fei B. Tumor detection of the thyroid and salivary glands using hyperspectral imaging and deep learning. Biomed Opt Express. 11(3):1383-1400.

Intraoperative Hyperspectral Imaging for Cancer Detection During Surgery in 36 Human Patients

Halicek M, Fabelo H, Ortega S, Little JV, Wang X, Chen AY, Callico GM, Myers LL, Sumer BD, Fei B. Deep Learning-Based Framework for In Vivo Identification of Glioblastoma Tumor using Hyperspectral Images of Human Brain. Sensors. 19(4):920.

UT DALLAS
The University of Texas at Dallas

UTSouthwestern
Medical Center

Augmented Reality and Hyperspectral Imaging-Guided Surgery

Pfefferle M, Shahub S, Shahedi M, …Fei B. Renal biopsy under augmented reality guidance. Proc SPIE Int Soc Opt Eng. 11315:113152W

Huang J, Halicek M, Shahedi M, Fei B. Augmented reality visualization of hyperspectral imaging classifications for image-guided brain tumor resection. Proc SPIE. 11315(113150U).

Fabelo H, Halicek M, Ortega S, …Fei B. Deep Learning-Based Framework for In Vivo Identification of Glioblastoma Tumor using Hyperspectral Images of Human Brain. Sensors;19(4):920

UT DALLAS
The University of Texas at Dallas

UTSouthwestern
Medical Center

The Operating Room of the Future

Bring Advanced Technology and Innovation to Surgery Patients

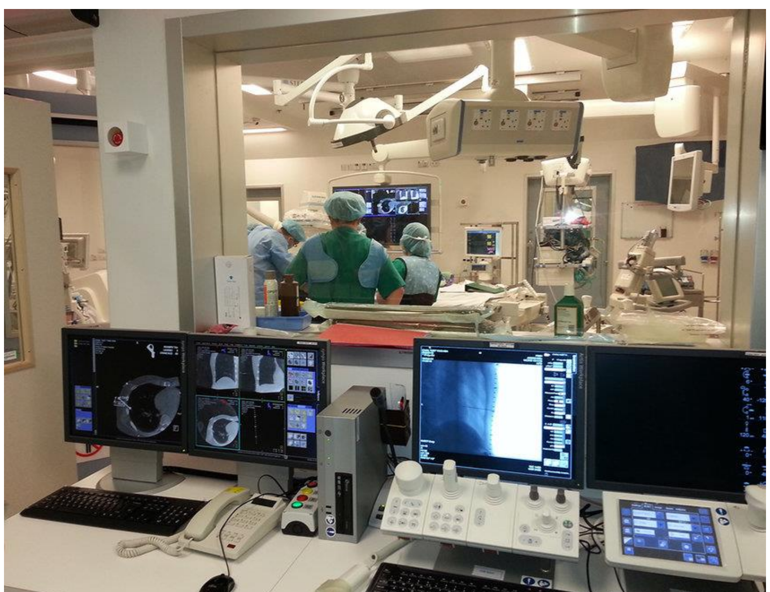

The Wall Street Journal and drwadegrindle.com

Discussions

- **Developed hyperspectral imaging methods for detecting H&N cancer in surgical specimens of 204 patients.**
- **Developed advanced image processing, quantification, and machine learning tools for hyperspectral data.**
- **Artificial intelligence will change the landscape of healthcare and imaging including biomedical optics.**
- **Hyperspectral imaging shows promising results for assessing tumor margins in surgical specimens and in *in vivo* image-guided surgery.**

Acknowledgements

Center for Imaging and Surgical Innovation (CISI)

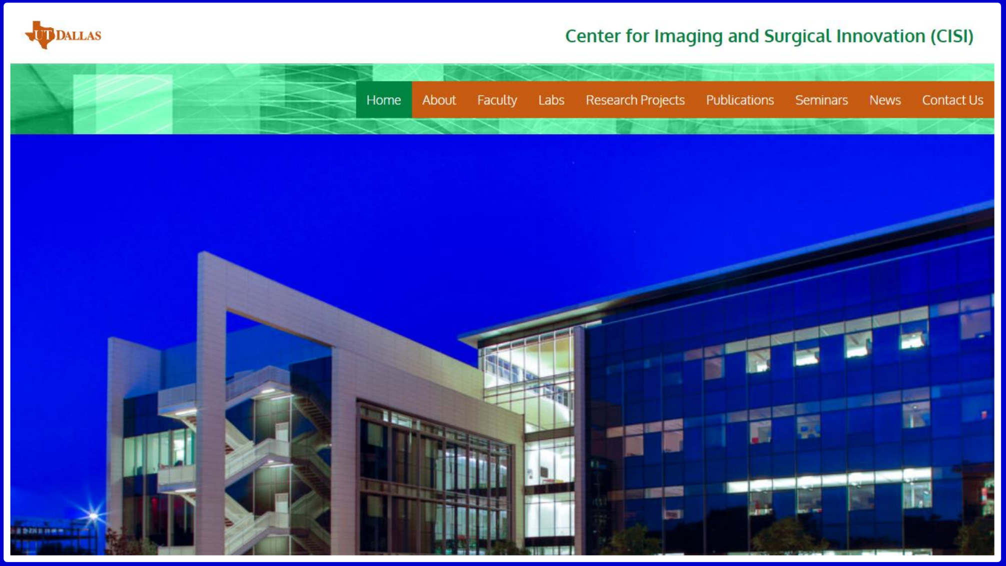

www.fei-lab.org

Funding Support: NIH CA204254, HL140124, CA231911, CPRIT RP190588

UT DALLAS The University of Texas at Dallas

UT Southwestern Medical Center